Dynamic and Transient Responses of a Low-Voltage DC Microgrid with Considering Multiple Battery-Supercapacitor-Based Energy Storage Configurations

Phuc Duy Le[1], Duong Minh Bui[2], Thanh Dung Nguyen[3]
Ho Chi Minh City University of Technology[1]
Vietnamese-German University (VGU)[2]
Cuu Long University (UCL)[3]
Vietnam

Abstract

This research presents experimental results of staged transient and dynamic operation tests for a low-voltage direct current microgrid (LVDC MG) with different energy-storage system (ESS) configurations. Photovoltaic-generation (PG) sources, batteries (BATTs), supercapacitors (SCs), DC-DC converters, and DC loads (DCLs) are connected through a point of common coupling (PCC) in an LVDC MG testbed to perform the staged-operation tests. Dynamic and transient operation cases of the LVDC MG prototype are performed respectively by supplying the PG power to the PCC and adjusting DC loads, and switching circuit breakers (CBs) to obtain the ESS's different behaviors for comparative assessments. In this point of view, the staged-operation tests are typically implemented in passive, semi-active, full-active, and separately-active configurations of the battery-supercapacitor (BATT-SC)-based hybrid ESS. Consequently, the full-active configuration of the BATT-SC ESS shows the outperforming results rather than the semi-active or passive configurations to quickly stabilize voltages and currents in different dynamic and transient operation cases of the off-grid LVDC microgrid.

1. Introduction

To achieve cleaner and more sustainable targets, and carbon dioxide emission reduction, the photovoltaic generation (PG) system is one of many forms of renewable energy sources (RESs) that is exploited to generate electrical power from solar energy [1-3]. This photovoltaic (PV)-generating system is highly appealing because of its broad application in both active and passive designs, which is beneficial for long-term strategies and has great potential in providing energy when compared to non-renewable sources [4,5]. However, the power output of the PV-generating sources is normally dynamic based on weather conditions despite applying maximum power point tracking (MPPT) techniques.

Energy storage systems (ESSs) could be implemented as an effective solution to absorb the excess energy from RESs, typically for the PG sources, or compensate the power shortage for the source-load power balance in the microgrid. The main configuration of ESS for PG applications is a battery energy storage system (BATT-ESS). In references [6-8], the efficiency increase of the ESS could be performed by combining both batteries (BATTs) and super-capacitors (SC) to form a hybrid energy storage system (HESS) that can mitigate shortcomings of the BATT-ESS in the microgrid.

The development of direct current microgrids (DCMGs) could be considered as a sustainable resolution for low-voltage DC distribution networks [9,10]. A DC MG consists of different elements such as local DC-power-generation sources, DC loads (DCLs), and energy storage devices which are interconnected through a point of common coupling (PCC) of the DC MG. Once disconnected from the utility grid, the DCMG will operate under an autonomous/islanded mode. In this islanded mode, the DC MG must be self-controlled to achieve the source-load power balance by applying the ESS to smoothly keep the DC voltage stable and absorb the excess energy from RESs or compensate for the power shortage in the DC MG. However, the ESS in the DC MG could be operated in several flexible configurations such as semi-active, full-active, passive, and separately-active configurations. Therefore, these ESS configurations should be more practically investigated under transient and dynamic operation conditions to provide valuable observations for selecting the most appropriate configuration to stabilize the DCMG voltage in the autonomous mode.

In general, this research aims to clearly understand transient and dynamic operation responses of multiple BATT-SC-based ESS configurations in the LVDC microgrid. Based on an LVDC MG test-bed with variable resistive loads and the random power change of PV-generating sources, staged transient and

 | DOI: 10.20533/ijsed.2046.3707.2021.0052

dynamic operation tests are performed respectively for each ESS configuration to obtain the voltage-stabilizing performance and the proper time-response. Novel contributions of this research are briefly listed as follows:

- Experimental results of voltage and current responses to transient and dynamic operations of three BATT-ESS, SC-ESS, and BATT-SC-ESS configurations in the LVDC MG testbed are analyzed and discussed in detail to select the most appropriate topology for the DCMG at the autonomous/islanded mode.
- Staged test results are compared to simulation results from PSCAD software for the practice-theory validation.
- For each ESS configuration, the time response of the voltage stabilization is assessed under transient and dynamic operation cases in the LVDC MG test-bed.

The organization of this paper is shown as follows. Section 2 introduces theoretical background related to the operation and control of the LVDC MG for doing staged transient and dynamic experiments. Section 3 presents a prototype of the LVDC MG. Details of the staged transient and dynamic operation tests of multiple proposed ESS configurations are mentioned in Section 4. Finally, conclusions and future works are given in Section 5.

2. Theoretical Background on the Operation and Control of LVDC MG with Different ESS Configurations

Recent research proposed multiple ESS configurations for the DC MG with PV-generating sources [11], [12]. It could be agreed that the energy storage system increases the microgrid's total efficiency and the power-supply reliability through dispatching power flows to DC loads and supporting the intermittent power output of PV-generating sources [12]. If the BATT-ESS is fully charged, the PG source will be operated at the constant power-generating mode in the DC microgrid. In contrast, the BATT-ESS is utilized whenever the output power of the PG source is insufficient or unavailable for the DC load demand. Moreover, the grid-connected operation mode is considered when the total amount of power from both the PG source and the BATT-ESS is not sufficient for the load demand. In addition, the super-capacitors (SC) can work as an energy storage system to endure many more cycles and allow a faster charging/discharging process when compared to the conventional BATTs. In reference [13], the main purpose of using the SCs is to provide a large amount of energy within a very short time, which is mostly adaptable for minimizing the power fluctuation of the PG sources in the DC MG and the battery deterioration.

According to references [14,15], the BATT-SC-based HESS is connected to a DC common bus in three passive, semi-active, and full-active topologies, as shown in Figure 1. In this research, four flexible ESS configurations, namely passive, semi-active, full-active, and separately-active configurations, are rigorously investigated to clearly understand their behaviors under transient and dynamic operation cases in an LVDC MG with PV-generating sources.

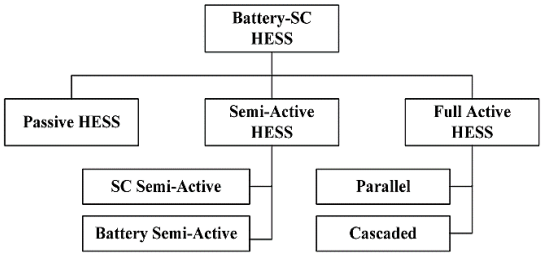

Figure 1. Classification of HESS topologies with the battery and supercapacitor devices

2.1. Semi-active and full-active HESS configurations

Figure 2 shows a semi-active HESS topology where either the super-capacitors or the batteries are connected to the DC common bus through power electronic converters, thus allowing the power flow of those components to be semi-actively controlled [16]. When only the super-capacitor is connected through the power converter, the semi-active HESS draws benefits from the super-capacitors which in turn improves the transient and dynamic performance of the DC MG, while the batteries ensure the stabilization of the DC bus voltage [17]. The shortcoming of this configuration is that the batteries are no longer protected from high currents caused by the transient and dynamic operations. Therefore, the battery's lifespan could be dramatically dropped [18].

A full-active HESS configuration is represented in Figure 3. Both the batteries and super-capacitors are connected to a common DC-bus through DC-DC power electronic converters to improve the performance and reliability of the entire system [18]. The parallel configuration allows the full control of both BATTs and SCs. In the cascaded configuration, the batteries are current-controlled, and the capacitors are voltage-controlled to regulate the DC-bus voltage of the microgrid. However, the full-active HESS topology introduces more DC-DC power converters to the system meaning more power losses due to the conversion efficiency as well as the reliability reduction of the whole system [19], [20].

For a passive configuration, the ESSs are simply connected to the DC common bus, unregulated by any power controller, as depicted in Figure 4. In this

 | DOI: 10.20533/ijsed.2046.3707.2021.0052

configuration, consideration of the voltage characteristics of the ESSs must be taken into account. On the other hand, a separately-active HESS configuration can use either BESS/SC or both at the same time to provide the power to the system. In this separately-active configuration, two separate power converters are used to regulate the power balance. In this case, a high-efficiency buck-boost converter is used to act as another power controlling unit, connecting a DC power source to the common bus.

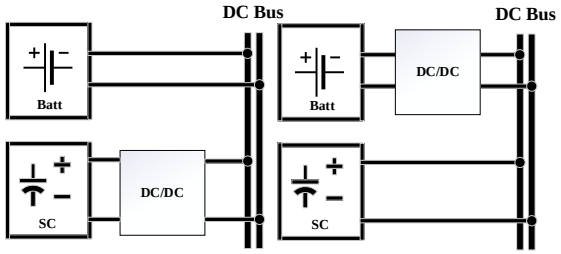

Figure 2. Semi-active HESS topologies (a) Super-capacitor-based semi-active HESS topology; and (b) Battery-based semi-active HESS topology

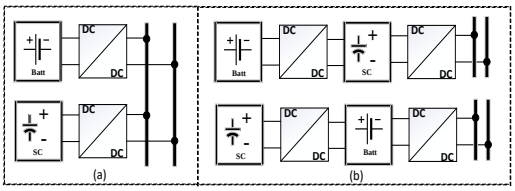

Figure 3. Full-active HESS topologies (a) the parallel-connected BATT and SC; and (b) the cascade-connected BATT and SC

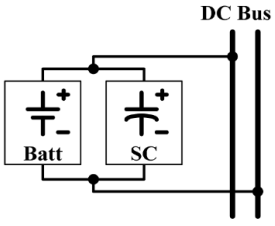

Figure 4. Passive HESS topology with the BATT and the SC connected in parallel

2.2. Non-isolated DC-DC bidirectional converter

The non-isolated bidirectional DC-DC converters (NIBDCs) do not employ isolated transformers; hence no galvanic isolation is presented between the source and the load. This type of power converter is suitable for small applications due to the lack of weight from the absence of transformers and is easier to control [21]. Table 1 shows the common non-isolated bidirectional DC-DC converter topologies and their operational characteristics. In this research, the authors select the first topology of the NIBDC in Table 1, i.e. a half-bridge bidirectional converter topology, for the staged transient and dynamic tests in the LVDC MG prototype due to its outperforming characteristics.

Table 1. Common non-isolated bidirectional DC-DC converter topologies and their operational characteristics*

Topology	Descriptions		
	$\frac{V_o}{V_i}$	Output current ripple	Characteristics
Half-bridge	$\frac{1}{1-D}$	$\frac{V_o(1-D)}{Lf_{sw}}$	A low number of elements, discontinuity of I_{in}
Cascaded bidirectional	$\frac{1}{1-D}$	$\frac{V_o\,(1-D)}{Lf_{sw}}$	Higher voltage gain, lower current stress
Ćuk	$\frac{-D}{1-D}$	$-\frac{V_i\,D}{L_2\,f_{sw}}$	Continuous currents I_{in} and I_{out}
SEPIC/ Zeta	$\frac{D}{1-D}$	$\frac{V_i\,D}{L_2\,f_{sw}}$	The positive output voltage, reduced current ripple
Switched capacitor	2	$Cf_{sw}(V_{in}-V_o)$	No inductor, continuous current I_{in}
Interleaved	$\frac{1}{1-D}$	$\frac{V_o(1-2D)}{Lf_{sw}}$	Low switching-frequency current ripple

*Note: *V_i and V_o are input and output voltages respectively; I_i and I_o are input and output currents respectively; D is the duty cycle; L and C are reactance and capacitance respectively; f_{sw} is switching frequency.*

2.3. Control strategies in a typical LVDC microgrid

The droop control method is commonly installed on top of inner loops for current-sharing purposes. Either the power output or the current output can be selected as the feedback signal in droop control.

$$v_{DCi} = v_{DC} - m_p \,.\, P_{oi} \quad (1)$$

$$v_{DCi} = v_{DC} - m_c \,.\, i_{oi} \quad (2)$$

Equation (1) is used for the constant-power load type in the microgrid and the output powers of the sources are considered as the droop feedback, while Eq. (2) is applied when the current signal is obtained. Droop coefficients m_p and m_c can be regarded as a virtual internal resistance which simplifies the implementation process with a linear function [22]. v_{DCi} is the output voltage of the *i*-th power converter. v_{DC} is the rated DC voltage value. P_{oi} is the output power of the *i*-th power converter and i_{oi} is the output current of the *i*-th power converter.

On the other hand, a decentralized control strategy is well-performed by local controllers in the

microgrid. Common decentralized control methods are the DC bus signaling (DBS) and the power line signaling (PLS). Their prominent advantages are not complex to implement and rely on digital communication. The DBS is the most prominent decentralized method for DC MGs [23,24]. The PLS is more complex to implement compared to other decentralized control methods, commonly used for changing the operating modes of the microgrid and cutting-off corrupted components while being unsuitable for the power-sharing in the microgrid. Therefore, the decentralized control method-DBS is used for DC-DC converter controllers of the LVDC MG prototype as mentioned in this research.

3. A 12V DC Microgrid Testbed and Staged Transient and Dynamic Tests

3.1. A 12V DC microgrid testbed

Table 2 illustrates all main components of the BATT-SC-based HESS in a real 12V DC MG testbed. In addition, a detailed experiment model is set up for staged transient and dynamic operation tests, as seen in Figure 5. Photovoltaic (PV) panels provide the power to the MPPT solar controller unit. Depending on how many volts the PV panels operate, the MPPT controller will adjust its operating mode. Through a DC circuit breaker-CB3, the MPPT solar controller is connected to the MPPT_DC block, which may contain both the BATT and SC devices acting as DC power sources. The MPPT solar controller is also connected to the PCC through the DC circuit breaker-CB2 in the system model.

In Figure 5, there is also an ISL block which can be left empty, have a passive DC power source, or contain the ISL81601 microcontroller, working as a DC-DC power converter with the SC for energy storage operations in the DC microgrid testbed. A current meter is connected in series with the Leybold's adjustable resistive loads (rheostats). A FLUKE data logging device will always be connected to the common DC bus. Due to a limited number of data logging devices, the remaining FLUKE will be connected to either MS1 or MS3, depending on staged test scenarios of the LVDC microgrid testbed.

Table 2. Main elements of a battery-supercapacitor-based hybrid energy storage system in a 12V DCMG testbed

No.	Description	Illustration figures
1	Leybold's synchronously adjustable and circular rheostats	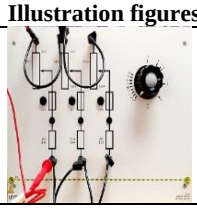
2	VLRA AGM Globe 12V – 7.5A	
3	16.5F supercapacitor banks	
4	Smart1 PV Charge Controller Data Sheet	
5	A Non-isolated Bidirectional DC-DC Converter: Renesas's ISL81601EVAL1Z with the built-in ISL81601 microcontroller	
6	Solar panels	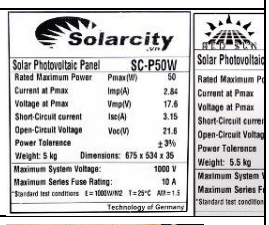
7	FLUKE's 437II Power and Energy Analyzer	

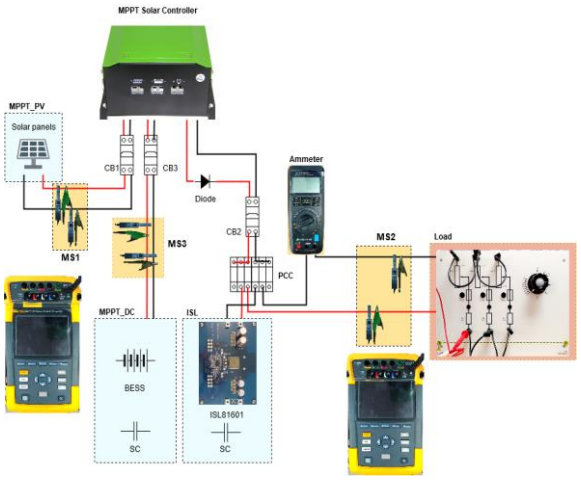

Figure 5. A typical experiment model of an off-grid LVDC microgrid testbed with a MPPT solar charge controller and the bidirectional DC-DC converter

A whole framework of staged tests is also given in Figure 6. There are six main steps to perform the proposed transient and dynamic operation tests on a 12-Volts DC MG prototype, including:

- Step 1: Set up a 12-Volts DC microgrid prototype/testbed using instruments shown in Table 2, and then check the residual-current-based safety.
- Step 2: Build a microgrid simulation model on the PSCAD software before the similarity comparison to the microgrid prototype. If they are matched, staged test scenarios will be then conducted corresponding to each wire-connection diagram.
- Step 3: Run the staged transient and dynamic operation tests, and capture the waveforms of each element of the LVDC MG prototype, as mentioned in Table 3. Similarly, it is needed to run simulation tests of the DCMG from the PSCAD software and record the test results.
- Step 4: Compare the staged experiment and simulation testing results; if they express the analogous behaviors, the results could be acceptable and then continue to the next scenarios; if not, it is needed to double-check the wiring connections of the microgrid prototype/PSCAD simulation model, or redo the staged experiment/simulation tests until their results are matched.
- Step 5: Repeat Step 3 and Step 4 until the "out-of scenarios" condition is satisfied.
- Step 6: Build a comparative result table to summarize all main observations and assessments that are obtained from staged experiments and simulation tests.

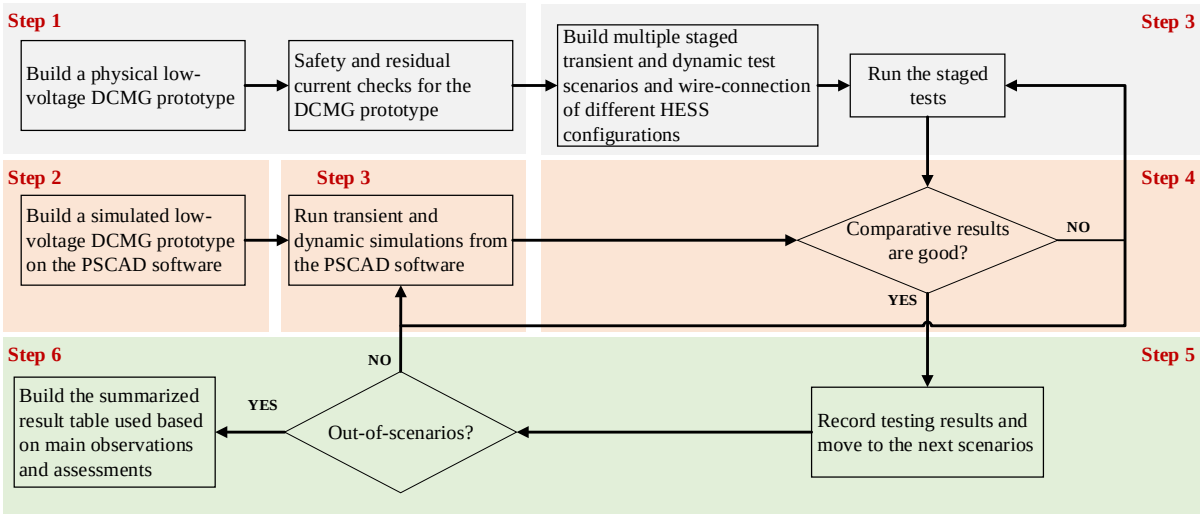

Figure 6. The whole framework of staged transient and dynamic operation tests of the LVDC MG testbed

3.2. Staged transient and dynamic tests of a 12V LVDC microgrid testbed

Overall, a total of nineteen scenarios were observed and had their data logged, which could be generalized according to four battery-supercapacitor-based ESS configurations, specifically i) the semi-active battery-supercapacitor-based ESS topology: two DC sources provide the power to the load, one is connected directly to the PCC of the system, and the other is connected to the PCC through a DC-DC converter; ii) the battery-supercapacitor-based ESS full-active topology: two DC sources provide the power to the load while both are controlled by a single DC-DC converter, iii) the passive ESS topology: energy storage devices are passively connected to the PCC of the system, not regulated by any type of power controller and iv) the separately-active ESS topology: two DC sources are controlled by two different power converters. One converter is integrated inside the MPPT solar charge controller, while the other is the high-efficiency buck-boost DC-DC converter, which only works with the supercapacitors.

Each battery-supercapacitor-based ESS topology has two operation solutions, specifically i) rheostats (R) for staged dynamic tests - the resistive load starts at 100%, then it is gradually lowered to 5% before returning to 100% in each case; and ii) the constant load with 5%R for staged transient tests - the resistive load starts at 5%, then CB1 is opened to cut off the PV-generating system (i.e. the MPPT_PV block as seen in Figure 5) completely from the MG. On the other hand, each aforementioned operation solution consists of multiple sub-tests for different ESS topologies, typically i) the only-BESS tests - only the batteries are present in the MG; ii) the only-SC tests - only the SCs are present in the MG; and iii) the both BESS and SC tests - both BATTs and SCs are present in the DC MG. Table 3 lists all the cases and which methods are used for field tests, along with the

 | DOI: 10.20533/ijsed.2046.3707.2021.0052

operation status of the related CBs as well as measurement (MS) points in the system. The detailed connections for each staged test scenario of the 12V DC MG testbed with the BATT-SC-based HESS are represented in Table 4. It is worth noting that there are minor differences between the experiment model and the simulation model. Simulation results from the PSCAD software are used for validating the staged experiment results of all possible HESS configurations in the 12V LVDC MG testbed.

Table 3. Staged transient and dynamic experiment/simulation scenarios of a 12V DC MG testbed having the BATT-SC-based HESS[*,**]

		MS1	CB1	MS2	CB2	MS3	CB3
Semi-Active ESS Configuration (Scenarios from 1 to 6)							
Rheo-stats	**BESS**	Yes	R-Closed	Yes	R-Closed	No	R-Closed
	SC						
	BESS-SC						
Con-stant 5%R	**BESS**	No	D-Opened			Yes	
	SC						
	BESS-SC						
		MS1	**CB1**	**MS2**	**CB2**	**MS3**	**CB3**
Full-Active ESS Configuration (Scenarios from 7 to 12)							
Rheo-stats	**BESS**	Yes	R-Closed	Yes	R-Closed	No	R-Closed
	SC						
	BESS-SC						
Con-stant 5%R	**BESS**	No	D-Opened			Yes	
	SC						
	BESS-SC						
		MS1	**CB1**	**MS2**	**CB2**	**MS3**	**CB3**
Passive ESS Configuration (Scenarios from 13 to 15)							
	BESS	No	R-Closed	Yes	D-Opened	No	R-Closed
	SC						
	BESS-SC						
		MS1	**CB1**	**MS2**	**CB2**	**MS3**	**CB3**
Separately Active ESS Configuration (Scenarios from 16 to 19)							
Rheostats	**SC**	Yes	R-Closed	Yes	R-Closed	No	R-Closed
	BESS-SC						
Con-stant 5%R	**SC**	No	D-Opened			Yes	
	BESS-SC						

*Note: *"D-open" means that the CB is opened after the data logging has started; "R-closed" means that the CB is always closed during the test case; and "Yes or No" means that which measurement system is taken for different experiments.*

***The configuration order denotes the controlled component. For example, in the "BESS-SC" scenario, the BESS is regulated by a controller, while the SC is passively connected to the system. In the "Separately Active ESS Configuration", all components are actively regulated by the controllers.*

Table 4. Detailed connections for each staged test scenario of the 12V DC MG testbed with the BATT-SC-based HESS configurations

Scenarios	Descriptions of wiring-connections in detail
1ST	A BATT device is present in the MPPT_DC block with PV arrays. Another BATT device is directly connected to the PCC. Measurements are taken at the MS1 and MS2 positions as seen in Figure 5. The resistive load is set to 100% at first. All CBs are closed. After the data has been logged for a few seconds, the resistive load is adjusted every second in the following order: 100% --> 80% --> 60% --> 40% --> 20% --> 10% --> 5% --> 100%. Once the common DC bus voltage has recovered, the data logging is stopped.
2ND	A SC bank is connected to the MPPT_DC block. Another SC bank is passively connected to the PCC of the microgrid testbed. The MPPT solar charge controller will not function without a BATT device, therefore, a BATT device is used to kick-start its initial operation. Once the MPPT controller is working normally, the BATT could be disconnected. The remaining steps are the same as the 1ST scenario.
3RD	For the BESS-SC combined scenario, the BESS is controlled by the solar charge controller while the SC device is passively connected to the PCC in the system.

 | DOI: 10.20533/ijsed.2046.3707.2021.0052

4TH	A BATT device is present in the MPPT_DC block and another BATT device replaces the ISL block as referred to Figure 5. Measurements are taken at two positions of MS3 (MPPT_DC) and MS2 (PCC). The resistive load is set at 5%R before the initiation of data logging. After a few seconds, CB1 is opened for around 1.5s to 2s, then CB1 has closed again. The data logging is stopped once the DC voltage at the positions of MS2 and MS3 have recovered and stabilized in the microgrid testbed.	
5TH	The SC banks replace the batteries from the BESS case. The resistive load should be reset to 100%R to allow the SC banks to fully charge first after kick-starting the off-grid microgrid system with another BATT device in the MPPT_DC block. Once both the SC banks are fully charged and the BATT device removed from the MPPT_DC block, the remaining steps are the same as the previous scenarios.	
6TH	A BATT device powers the MPPT_DC block while a SC device is connected passively to the PCC.	
7TH	A single BATT device is present in the MPPT_DC block. The PCC does not have any additional DC power source connected to it. Measurements are taken at the positions of MS1 and MS2. The remaining steps are the same as the 1ST scenario.	
8TH	A SC bank replaces the BATT inside the MPPT_DC block. A BATT device is needed to kick-start the MPPT solar charge controller.	
9TH	Both the BATT module and the SC bank are integrated inside the MPPT_DC block. Since a BATT device is already connected to the MPPT Controller, a kick-start is not needed. If the MPPT Solar Controller is stuck at checking voltage input, temporarily removing the SC bank will allow the controller to boost up normally.	
10TH	A BATT device is present in the MPPT_DC block. No DC-power source is provided at the PCC of the microgrid testbed. Measurements are taken at the positions of MS2 and MS3. The remaining steps are the same as section 5TH scenario.	
11TH	A SC bank replaces the BATT in the MPPT_DC block. A kick-start using a VLRA BESS at CB3 is needed for the controller to operate normally.	
12TH	Both the BATT and the SC bank are integrated into the MPPT_DC block of the MG testbed	
13RD	A BATT device is passively connected to the PCC (inside the ISL block as referred in Figure 5).	Once the ESS is fully charged and the system is running at the steady-state, CB2 has opened to completely cut off the PV power source from the microgrid testbed. After a few seconds, CB2 is closed again to restore the steady-state operation.
14TH	A supercapacitor unit is passively connected to the PCC (inside the ISL block as referred in Figure 5).	
15TH	Both the BATT and the supercapacitor are passively connected to the PCC (inside the ISL block as referred in Figure 5).	
16TH	This scenario uses purely the SCs to power the system. For this reason, a kickstart using 12V VLRA is needed for the MPPT solar charge controller.	The ISL810601 microcontroller is used for these testing scenarios, which activates the ISL block in Figure 5 to provide the backup power to the LVDC microgrid system in case of faults occurred at the PV arrays or the ESS configuration.
17TH	The MPPT_DC block uses a BATT device to power the MPPT solar charge controller, while the ISL block contains the ISL81610 microcontroller to regulate the charge and discharge or a supercapacitor unit.	
18TH	This scenario uses purely the SC to power the system.	
19TH	The MPPT_DC block uses a BATT device to power the MPPT solar charge controller, while the ISL block contains the ISL81610 microcontroller to regulate the charge and discharge or a supercapacitor unit.	

4. Results, Analysis and Discussion

Dynamic and transient testing results of the 12V LVDC MG testbed with different ESS topologies are given in Table 5 and from Figure 7 to Figure 23 along with the detailed analysis and discussion. Additionally, Table 6 gives a summary based on the staged transient and dynamic operation tests of the MG testbed. By considering various test scenarios with the semi-active ESS configurations, the power balance in the MG is controlled by the charging/discharing process of the ESS through the bidirectional DC-DC converter or the direct charge/discharge of the ESS to the PCC of the microgrid. This could be seen by comparing the current at the PCC of the DC MG among different semi-active rheostats cases. For the full-active ESS configurations, one controller is dedicated for controlling the output of ESSs, moreover, the integration of SCs into the system can immediately reduce voltage dips, and provide a fast time-response for the system voltage stabilization.

 | DOI: 10.20533/ijsed.2046.3707.2021.0052

Table 5. Staged transient and dynamic testing results of the 12V DC MG testbed with the BATT-SC-based HESS configurations

<table>
<tr><th>Cases</th><th colspan="2">Staged testing results</th><th>Analysis and discussion of obtained experiment results</th></tr>
<tr><td rowspan="4">1ST</td><td colspan="2"> 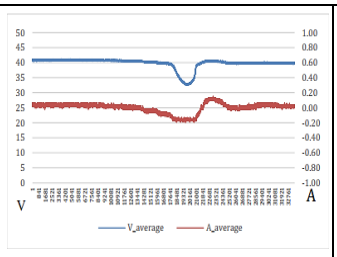 </td><td rowspan="4">Figure 7 shows that the changes are made at the resistive load causing both the voltage and current instability to the MPPT_PV. The current decreased when the resistive load was changed from 100% to 10%. Only after the load had been set to 5%R that the PCC current is increased again. A closer inspection under instantaneous waveform events shows that the current at the DC common bus was negative until the resistive load reached 5%R. This could be due to the passive DC source connected to the PCC without any converter, and it was assumed that the rest of the cases under semi-active would have similar responses.</td></tr>
<tr><td>(a) The measured V and I values at the MPPT_PV block</td><td>(b) The measured V and I values at the PCC of the MG</td></tr>
<tr><td colspan="2">Figure 7. Rheostats scenario results when using the semi-active BATT-based ESS topology.</td></tr>
<tr><td colspan="2"></td></tr>
<tr><td rowspan="4">2ND</td><td colspan="2"> 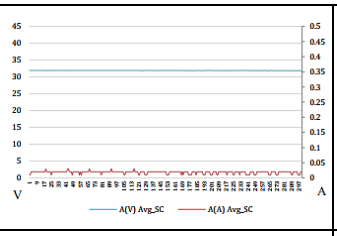 </td><td rowspan="4">Referred to Figure 8, it is shown that the current at the PCC would be negative until the resistive load reached 5%R. A prominent difference is that the voltage value at MPPT_PV was kept very stable with the introduction of SCs. Note that the PCC voltage is now 11.25V compared to BESS's 12.6V. This is consistent with simulation results where the PCC's voltage is the same as its parallel elements.</td></tr>
<tr><td>(a) The measured V and I values at the MPPT_PV block</td><td>(b) The measured V and I values at the PCC of the MG</td></tr>
<tr><td colspan="2">Figure 8. Rheostats scenario results when using the semi-active SC-based ESS topology.</td></tr>
<tr><td colspan="2"></td></tr>
<tr><td rowspan="4">3RD</td><td colspan="2"> 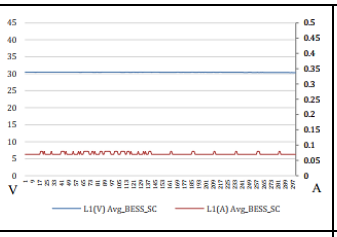 </td><td rowspan="4">When the SC device is used, the voltage and current responses at the PCC is faster, but also dips more than in the other cases. The MPPT_PV voltage and current are kept stable for SC, BESS_SC, and SC_BESS topologies, as referred to Figure 9.</td></tr>
<tr><td>(a) The measured V and I values at the MPPT_PV block</td><td>(b) The measured V and I values at the PCC of the MG</td></tr>
<tr><td colspan="2">Figure 9. Rheostats scenario results when using the semi-active BATT-SC-based ESS topology.</td></tr>
<tr><td colspan="2"></td></tr>
<tr><td rowspan="4">4TH</td><td colspan="2"> 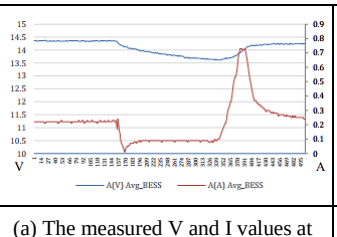 </td><td rowspan="4">Figure 10 shows that the MPPT_DC block acts as a positive current charging unit when the MPPT_PV block was still connected to the system. As soon as the MPPT_PV was disconnected, the BESS responded for a split second then normalized back to its current-sinking state. An interesting assumption is that the BESS connected passively to the PCC was</td></tr>
<tr><td>(a) The measured V and I values at the MPPT_DC block</td><td>(b) The measured V and I values at the PCC of the MG</td></tr>
<tr><td colspan="2">Figure 10. Constant 5% R scenario results when using a semi-active BATT-based ESS configuration.</td></tr>
<tr><td colspan="2"></td></tr>
</table>

 | DOI: 10.20533/ijsed.2046.3707.2021.0052

		providing enough the power to stablize the DC bus voltage.
5TH	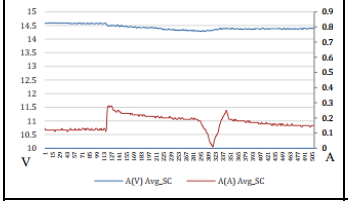 (a) The measured V and I values at the MPPT_DC block 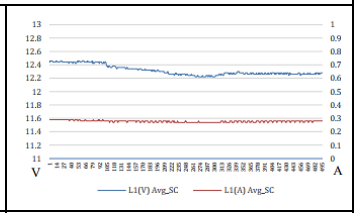 (b) The measured V and I values at the PCC of the MG **Figure 11.** Constant 5% R scenario results when using a semi-active SC-based ESS configuration.	As shown in Figure 11, when the MPPT_PV block was disconnected from the MG system, the SC responded immediately and became a power source. This current sourcing state was kept until the MPPT_PV block was reconnected.
6TH	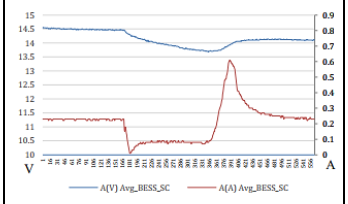 (a) The measured V and I values at the MPPT_DC block 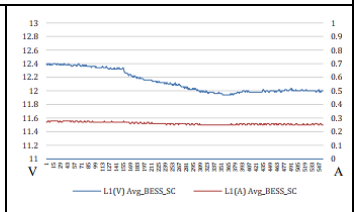 (b) The measured V and I values at the PCC of the MG **Figure 12.** Constant 5% R scenario results when using the semi-active BATT-SC-based ESS configuration.	The response in the BESS_SC case is similar to that of the BESS, except that the voltage in the PCC was dropping more rapidly, as seen in Figure 12.
7TH	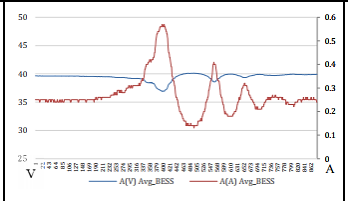 (a) The measured V and I values at the MPPT_PV block 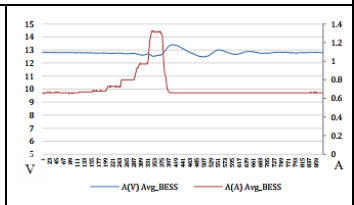 (b) The measured V and I values at the PCC of the MG **Figure 13.** Rheostats scenario results when using the full-active BATT-based ESS configuration.	At a glance, the changes in the PCC's load also result in the changes in the MPPT_PV block. The increase in the PCC's current also affects the MPPT_PV's block. When the load returns to 100%R, the voltage at the MPPT_PV experiences a high fluctuation before returning to its near original value. With the average value of 39.62V before dropping down to its lowest value of 36.90V (93.13%) and highest value at 40.14V (101.31%). The same happens to the PV current, except with much more pronounced fluctuation, as seen in Figure 13.
8TH	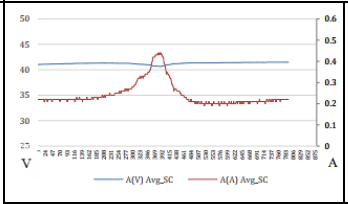 (a) The measured V and I values at the MPPT_PV block 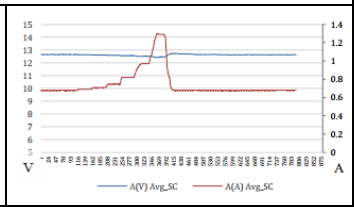 (b) The measured V and I values at the PCC of the MG **Figure 14.** Rheostats scenario results when using the full-active SC-based ESS configuration.	Compared to the case of BESS, the use of SCs has produced results with fewer overshootings and generally the improved dynamic response time of voltage and current for both the MPPT_PV block and the PCC in the DC MG testbed. The voltage values were maintained well within 2% tolerance, as shown in Figure 14.
9TH	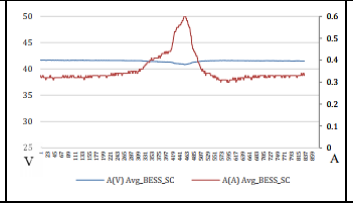 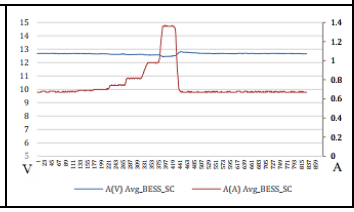	In case of using the SC and the combination of BESS and SC, it can give more deviation in the current at the steady state, but again, they are all kept within 2% tolerance. Figure 15 shows dynamic and transient

	(a) The measured V and I values at the MPPT_PV block	(b) The measured V and I values at the PCC of the MG
	Figure 15. Rheostats scenario results when using the full-active BATT-SC-based ESS configuration.	
		results when using the full-active BATT-SC-based ESS configuration. It could be generally concluded that the integration of SCs into the MG system is useful to regulate the voltage at the PCC, as illustrated in Figure 15.
10TH	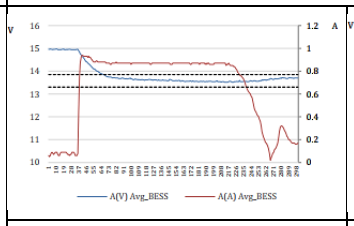	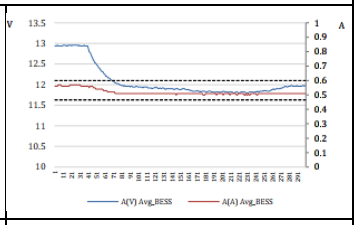
	(a) The measured V and I values at the MPPT_DC block	(b) The measured V and I values at the PCC of the MG
	Figure 16. Constant 5% R scenario results when using the full-active BATT-based ESS configuration.	
		Figure 16 shows a massive current increase when the MPPT_PV block was cut off from the system. Moreover, the voltage at the PCC decreased from 12.94V to 11.8V before recovering to 11.98V. The current at the PCC was kept nearly constant, the same cannot be said about the voltage. The MG system took some time to reach its 2% tolerance boundary.
11TH	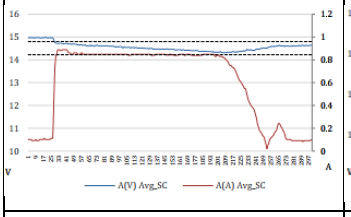	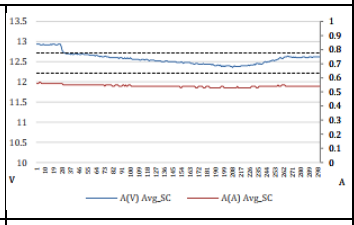
	(a) The measured V and I values at the MPPT_DC block	(b) The measured V and I values at the PCC of the MG
	Figure 17. Constant 5% R scenario results when using the full-active SC-based ESS configuration.	
		Figure 17 shows the voltage and current responses in case of using the full-active supercapacitor-based ESS configuration, which are mostly the same compared to the case of using the full-active BATT-based ESS configuration. It can be concluded that at both the MPPT_DC block and the PCC, the integration of SCs into the MG can reduce the voltage drop and shorten the dynamic response time. This can also lead to an effective voltage recovery without any noticeable underdamping effect.
12TH		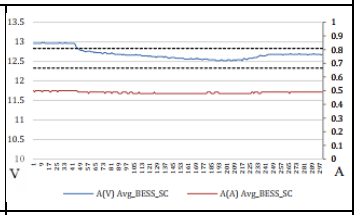
	(a) The measured V and I values at the MPPT_DC block	(b) The measured V and I values at the PCC of the MG
	Figure 18. Constant 5% R scenario results when using the full-active BATT-SC-based ESS configuration.	
		An interesting phenomenon happens once the BESS and the SC are put together, as shown in Figure 18, under the constant 5%R method and the full-active HESS configuration. After the MPPT_PV block had been reconnected to the system, the system is controlled to balance the source-load power distribution. Both the BESS and the SC are operated to reach the steady state of the DC microgrid. From the logged data, it is observable that the stability and dynamic response time of the voltage are both improved significantly with the utilization of SC into the system, connected in parallel with the BESS.

 | DOI: 10.20533/ijsed.2046.3707.2021.0052

13RD
14TH
15TH

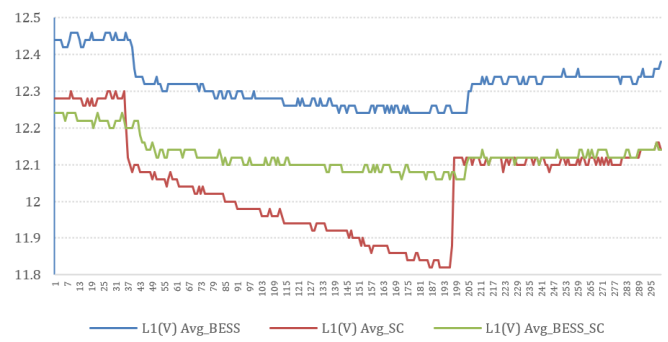

Figure 19. Dynamic voltage responses of the BESS-, SC-, and BESS-SC-based ESS configurations at the PCC.

It can be observed that dynamic response times of the PCC voltage are roughly the same for the BESS, SC, and BESS-SC ESS configurations. In the higher resolution, it is revealed that the voltage drop of the BESS is 1 sample faster while recovering 1 sample slower. As for the SC, the voltage naturally drops faster than BESS, as referred to Figure 19.

16th

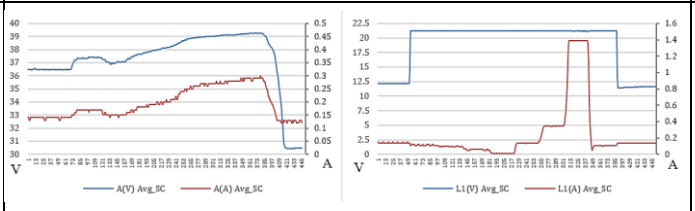

(a) The measured V and I at MPPT_PV block

(b) The measured V and I values at the PCC of the MG

Figure 20. Rheostats scenario results when using the separately active SC-based ESS configuration.

Figure 20 shows the RMS values of V and I captured at two different positions, the MPPT_PV block and the PCC. At the PCC, the voltage value is boosted from approximately 12.4V to 21.5V after the activation of the ISL81601 microcontroller.

17th

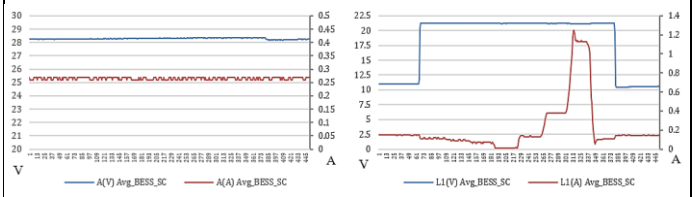

(a) The measured V and I values at MPPT_PV block

(b) The measured V and I values at the PCC of the MG

Figure 21. Rheostats scenario results when using the separately active BESS-SC-based ESS configuration.

With the integration of the BESS into the MPPT_DC block along with the SC, the voltage and current at the MPPT_PV block are stabilized as seen in Figure 21. At the PCC of the MG, the voltage and current responses are mostly improved in stabilization.

18th

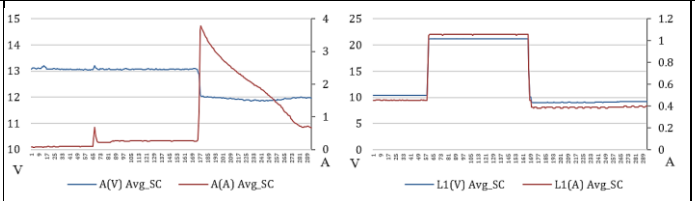

(a) The measured V and I values at MPPT_DC block

(b) The measured V and I values at the PCC of the MG

Figure 22. Constant 5% R scenario results when using the separately active SC-based ESS configuration.

Both Figure 22 (a) and Figure 22 (b) show the RMS values of voltage and current at the positions of the MPPT_DC block and the PCC of the microgrid. Wave events at the MPPT_DC block show that before and during the dynamic power fluctuation of the PV arrays, the MPPT_DC block with the presence of SCs was consuming a small amount of residual power. Only after reconnecting the solar arrays and switching the ISL81601 controller to the charging mode, the MPPT_DC block would begin to provide the power back to the DC common bus of the microgrid testbed.

 | DOI: 10.20533/ijsed.2046.3707.2021.0052

19th	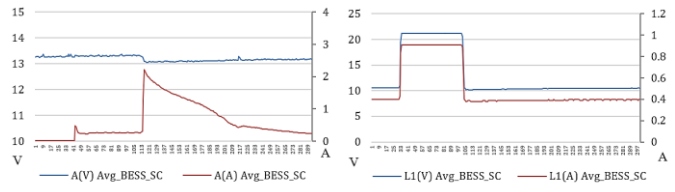	With the integration of both the BESS and the SC into the MPPT_DC block, the current surge is reduced almost by half the value in comparision wih only the integration of the SC to the MPPT_DC block, as referred to Figure 23.
	(a) The measured V and I values at MPPT_DC block / (b) The measured V and I values at the PCC of the MG	
	Figure 23. Constant 5% R scenario results when using the separately active BESS-SC-based ESS configuration.	

Table 6. Summary of main observations from staged dynamic and transient testing results of the 12V DC MG

Semi-active ESS topologies		**Observed results**	
Rheostat loads	BESS	Voltage instability at both the load side and the source side; the slow dynamic response time; and the passive element dominates the charge/discharge routine until the load is high enough.	
	SC	Significantly improved stability at the source side; and there is no noticeable instability at the load side of the 12V DC MG testbed.	
	BESS_SC		
	SC_BESS		
Constant 5%R loads	BESS	A high current spike at the reconnection time of DC-power sources to the DC MG testbed.	
	BESS_SC		
	SC	A subdued current spike at the reconnection time of DC-power sources to the system; and the reduced voltage drops at both the sources and the loads in the system.	
	SC_BESS		
Full-active ESS topologies		**Observed results**	
Rheostats	BESS	Severe voltage and current fluctuations at the source and load sides; very slow response time with high overshootings and undershootings.	
	SC	No voltage or current fluctuations; significantly improved stability; and the very fast dynamic and transient response time.	
	BESS_SC	No voltage or current fluctuations; significantly improved stability; and the fast dynamic and transient response time.	
Constant 5%R	BESS	Slow response time; and the high current fluctuation at the source side.	
	SC	Significantly improved dynamic/transient response time; and the high current fluctuation at the source side.	
	BESS_SC	Improved response time; and the reduced current ripples at the source side.	
Passive ESS topologies		**Observed results**	
BESS		Reduced voltage drops.	
SC		Reduced voltage drops with slightly faster response time.	
BESS_SC		Reduced voltage drops with slightly faster response time; and the voltage drop rate according to DC-power sources.	
Separately-active ESS topologies		**Observed results**	
Rheostats	SC	Instability at the PV-generating source	Stable load voltage; ultra-fast dynamic and transient response times, e.g. voltage rise/fall time of no more than 4ms;
	BESS_SC	The PV-generating source is stabilized.	
Constant 5%R	SC	High current surge at the MPPT_DC block	
	BESS_SC	The reduced current surge at the MPPT_DC block	

 | DOI: 10.20533/ijsed.2046.3707.2021.0052

5. Conclusion

Experiment and simulation results of multiple battery-supercapacitor-based ESS configurations under staged dynamic and transient tests of a LVDC MG testbed have been analyzed and discussed in this research. To perform the staged tests, a LVDC MG prototype was built with PV-generating sources, BATTs, SCs, buck-boost DC-DC converters, and DCLs interconnected through a PCC. By doing the PG power injection, changing resistive loads, and switching circuit breakers, transient and dynamic behaviors of the ESS configurations have been obtained for comparative assessments. The staged tests are performed with possible battery-supercapacitor-based HESS configurations, such as semi-active, full-active, passive, and separately-active topologies. As a result, the full-active topology of BATT-SC-based ESS shows outperforming results rather than the semi-active ESS configuration when quickly responding to get the voltage stabilization under dynamic/transient operation cases of the off-grid LVDC microgrid. Using the full-active ESS topology also results in numbers and graphs that are intuitive to read and analyze, while using the microcontrollers gives the ultra-fast system response times and stabilizes the system quickly if the microcontroller can be configured properly. In the process of achieving these goals, the research also indicates main observations as the following.

- Without any type of power controller, the DC common bus follows the voltage value of its passive DC-power sources. When there is a possible combination of two different energy storage sources, they trickle the charge and discharge for each other while also providing power to the load. This means the most stable passive element determines the response of the microgrid system.
- Passive DC-power sources would provide the passive power to the PCC causing the system to negate a large portion from the active DC-power source. Only when the load was high enough that the system would pool both active and passive elements together.
- For most experimental and simulation cases, the integration of SCs to the DC microgrid system could provide the improved voltage stability to the previously unstable responses.
- Active DC-power sources with the combinational use of SCs, BESSs, and power converters can provide a near-instant response to the spikes in dynamic loads. Furthermore, dynamic exchanges between DC-power sources were observed, yet the voltage at the PCC was kept mostly stable in the DCMG.

6. References

[1] P. Mann, L. Gahagan, and M. B. Gordon, “Tectonic setting of the world's giant oil and gas fields,” in Michel T. Halbouty (ed.) Giant Oil and Gas Fields of the Decade, Tulsa, Okla, American Association of Petroleum Geologists, pp. 50, 1990–1999.

[2] D. M. Bui, P. D. Le and T. D. Nguyen, "Staged Fault Tests to Validate a Fast Protection System of Low-Voltage DC Microgrids," 2021 International Conference on Electrical, Computer, Communications and Mechatronics Engineering (ICECCME), pp. 1-6, 2021, doi: 10.1109/ICECCME52200.2021.9591112.

D. Bui, C. Wu, S. Chen, C. Huang and K. Lien, "Installation on a community-sized DC microgrid system and suggestion on a DC short-circuit test procedure," 2014 China International Conference on Electricity Distribution (CICED), Shenzhen, China, pp. 1819-1825, 2014, doi: 10.1109/CICED.2014.6992266.

[3] “Solar Energy Perspectives: Executive Summary,” International Energy Agency, 2011.

[4] Morton, Oliver, "Solar energy: A new day dawning? Silicon Valley sunrise," Nature, 443 (7107): 6 pp. 19–22, September 2006.

[5] M. Mangaraj, A. K. Panda and T. Penthia, "Supercapacitor supported DSTATCOM for harmonic reduction and power factor correction," 2016 IEEE Students' Conference on Electrical, Electronics and Computer Science (SCEECS), Bhopal, pp. 1-6.

[6] M. Farhadi and O. Mohammed, "Adaptive Energy Management in Redundant Hybrid DC Microgrid for Pulse Load Mitigation," in IEEE Transactions on Smart Grid, vol. 6, no. 1, pp. 54-62, Jan 2015.

[7] M. Farhadi and O. Mohammed, "Performance enancement of actively controlled hybrid DC microgrid with pulsed load," 2014 IEEE Industry Application Society Annual Meeting, Vancouver, BC, pp. 1-8, 2014.

[8] Ravichandran, Adhithya and Malysz, Pawel and Sirouspour, Shahin and Emadi, Ali, “The critical role of microgrids in transition to a smarter grid: A technical review,” pp. 1-7, 2013.

[9] T. M. I. Mahlia, T. J. Saktisahdan, A. Jannifar, M. H. Hasan, H. S. C. Matseelar, “A review of available methods and development on energy storage; technology update,” Renewable and Sustainable Energy Reviews. 33, pp. 532–545, 2014.

[10] Bhargavi, K. and N. S., Jayalakshmi and Gaonkar, Dattatraya and Shrivastava, Ashish and Jadoun, Vinay, “A Comprehensive Review on Control Techniques for Power Management of Isolated DC Microgrid System Operation,” IEEE Access. pp. 1-1, 2021.

[11] Dragicevic, Tomislav, Lu, Xiaonan, Vasquez, Juan C., Guerrero, Josep.. DC Microgrids–Part I: A Review of Control Strategies and Stabilization Techniques. IEEE Trans. on Power Elec. 31, 2015, 1-1.

[12] Z. Tehrani, D. J. Thomas, T. Korochkina, C. O. Phillips, D. Lupo, S. Lehtimäki, J. O'Mahony, and D. T Gethin, "Large-area printed supercapacitor technology for low-cost domestic green energy storage," Energy. 118, pp. 1313–1321, 2017.

[13] A. Kuperman, I. Aharon, “Battery-ultracapacitor hybrids for pulsed current loads: A review,” Renew Sustain Energy Rev, 15, (2), pp. 981–992, 2011.

 | DOI: 10.20533/ijsed.2046.3707.2021.0052

[14] T. Ma, H. Yang and L. Lu, “Development of hybrid battery-supercapacitor energy storage for remote area renewable energy systems,” Appl Energy, 153, pp. 56-62, 2015.

[15] Ziyou Song, Heath Hofmann, Jianqiu Li, Xuebing Han, Xiaowu Zhang, and Minggao Ouyang, “A comparison study of different semi-active hybrid energy storage system topologies for electric vehicles,” Journal of Power Sources, Volume 274, pp. 400-411, 2015, ISSN 0378-7753.

[16] W. Li and G. Joos, "A power electronic interface for a battery supercapacitor hybrid energy storage system for wind applications," 2008 IEEE Power Electronics Specialists Conference, Rhodes, pp. 1762-1768, 2008.

[17] A. Etxeberria, I. Vechiu, H. Camblong, J.-M. Vinassa, “Comparison of three topologies and controls of a hybrid energy storage system for microgrids,” Energy Conversion and Management, Volume 54, Issue 1, ISSN 0196-8904, pp. 113-121, 2012.

[18] Chang Ye, Shihong Miao, Qi Lei and Yaowang Li, "Dynamic Energy Management of Hybrid Energy Storage Systems with a Hierarchical Structure," Energies, vol. 9(6), pages 1-15, May 2016.

[19] F. Ciccarelli, G. Clemente, and D. Iannuzzi, "Energy storage management control based on supercapacitors using a modular multilevel inverter topology for electrical vehicles," 2013 International Conference on Clean Electrical Power (ICCEP), Alghero, pp. 170-176, 2013.

[20] B. M. Reddy and P. Samuel, "A comparative analysis of non-isolated bi-directional dc-dc converters," 2016 IEEE 1st International Conference on Power Electronics, Intelligent Control and Energy Systems (ICPEICES), Delhi, pp. 1-6, 2016.

[21] “REbus DC Microgrid.” [Online]. Available: http://rebuspower.com/technical.shtml. Access Date: July, 2020.

[22] K. Sun, L. Zhang, Y. Xing and J. M. Guerrero, "A Distributed Control Strategy Based on DC Bus Signaling for Modular Photovoltaic Generation Systems With Battery Energy Storage," in IEEE Transactions on Power Electronics, vol. 26, no. 10, pp. 3032-3045, Oct. 2011.

[23] J. Schonbergerschonberger, R. Duke and S. D. Round, "DC-Bus Signaling: A Distributed Control Strategy for a Hybrid Renewable Nanogrid," in IEEE Transactions on Industrial Electronics, vol. 53, no. 5, pp. 1453-1460, Oct. 2006.

7. Acknowledgements

The authors would like to thank Mr. Hieu N.M. from Vietnamese-German University (VGU), Vietnam for implementing the staged transient and dynamic operation tests of the 12V DCMG testbed.

 | DOI: 10.20533/ijsed.2046.3707.2021.0052